



Effects of non-isothermal annealing on microstructure and mechanical properties of severely deformed aluminum samples: Modeling and experiment

A. R. KHODABAKHSHI, M. KAZEMINEZHAD

Department of Materials Science and Engineering, Sharif University of Technology, Azadi Avenue, Tehran, Iran

Received 25 July 2018; accepted 24 December 2018

Abstract: In order to investigate the evolution of microstructure and flow stress during non-isothermal annealing, aluminum samples were subjected to strain magnitudes of 1, 2 and 3 by performing 2, 4 and 6 passes of multi-directional forging. Then, the samples were non-isothermally annealed up to 150, 200, 250, 300 and 350 °C. The evolution of dislocation density and flow stress was studied via modeling of deformation and annealing stages. It was found that 2, 4 and 6 passes multi-directionally forged samples show thermal stability up to temperatures of 250, 250 and 300 °C, respectively. Modeling results and experimental data were compared and a reasonable agreement was observed. It was noticed that 2 and 4 passes multi-directionally forged samples annealed non-isothermally up to 350 °C have a lower experimental flow stress in comparison with the flow stress achieved from the model. The underlying reason is that the proposed non-isothermal annealing model is based only on the intragranular dislocation density evolution, which only takes into account recovery and recrystallization phenomena. However, at 350 °C grain growth takes place in addition to recovery and recrystallization, which is the source of discrepancy between the modeling and experimental flow stress.

Key words: severe plastic deformation; multi-directional forging; non-isothermal annealing; dislocation density-based model; microstructure; mechanical properties

1 Introduction

Multi-directional forging (MDF) is a way for producing ultra-fine grained materials by imposing severe plastic deformation. The study of annealing behavior of multi-directionally forged material is of great interest in order to improve the ductility without losing the strength achieved through MDF. Several studies focused on investigating the isothermal and isochronal annealing behavior of ultrafine grained commercial purity aluminum fabricated by imposing high amount of deformation and different kinds of phenomena were observed [1–13]. It was reported that annealing of ultrafine grained aluminum at low temperatures results in the rearrangement of dislocations, and cell structure formation which increases the strength of the materials [1,2]. Also, it was seen that annealing at higher temperatures leads to a recovered microstructure [3–8]. It was observed that the recovery rate is increased with increasing the amount of deformation [4,8] leading to the increase in apparent activation energy during

recovery [7,8]. In some cases, the lamellar structure of highly deformed material was reported to evolve into a more equiaxed structure during recovery under a mechanism called triple junction motion (TJM) which affects subsequent recrystallization [6–8]. There are also reports of recrystallization by further annealing highly deformed commercial purity aluminum at higher temperatures. The recrystallized microstructure was reported to be the result of various recrystallization mechanisms, such as discontinuous recrystallization [3,4,7], continuous recrystallization [9,10] and a mixed process, with some part of the microstructure showing a discontinuous recrystallization and elsewhere a continuous coarsening [11,12]. Moreover, the thermal stability of highly deformed aluminum was mentioned to be up to 275 °C [3,4,9,13].

In the case of non-isothermal annealing, researchers focused on the behavior of cold worked aluminum alloys which were under subsequent non-isothermal annealing. It was shown that reducing heating rate in non-isothermal annealing decreases the driving force for

recrystallization, causes recovery to happen and delays recrystallization. Also, higher heating rate leads to a smaller and more equiaxed recrystallized microstructure [14–19]. It was reported that during non-isothermal annealing, an increase in temperature within low temperature ranges and at constant low heating rates causes mechanical properties to reduce gradually, which is the consequence of recovery of microstructure. Further annealing up to higher temperatures results in recrystallization which reduces mechanical properties noticeably [20–24].

Nowadays, due to the improvement of computer technologies, computer modeling and simulations can be considered as good complements for experimental approaches. A dislocation density-based model called ETMB (Estrin, Toth, Molinari, Brechet) is widely used in Refs. [25,26] for investigating the deformation behavior of highly deformed materials. This model was firstly proposed by ESTRIN et al [25] for a two-dimensional state, and later it was generalized to the three-dimensional state [26]. ETMB model investigates dislocation density evolution by considering material as a two-phase composite which consists of cell interiors and cell walls and taking into account the evolution of dislocation density in each of the two considered phases.

Unlike recrystallization, there are only a few number of studies presenting a model for recovery during non-isothermal annealing, none of which is based on dislocation density evolution. KUHLMANN et al [27] proposed one of the first models for isothermal recovery by considering evolution of flow stress. Later, NES [28] introduced a more mechanistic model by approximating integrals of rate equations originated from Kuhlmann model. Also, BORELIUS et al [29] presented an isothermal recovery model based on relaxation of the stored energy of deformation. HANSEN et al [30–32] later successfully adopted this model for highly deformed commercial purity aluminum by changing the variables studied and investigating the evolution of unrecovered fraction of material instead of stored energy. SUMMERS et al [33] changed the isothermal recovery model introduced by HANSEN et al [30–32] into a non-isothermal recovery model by applying slight modifications and using some assumptions, so that it could be applicable over a range of temperatures rather than discrete isothermal exposures.

In this study, experimental procedure and modeling description and procedure were discussed in Sections 2 and 3, respectively. Then, in Section 4, the microstructural evolution was investigated and the ETMB model was used to predict the flow stress evolution of commercial purity aluminum deformed through different passes of multi-directional forging. In the following a model was introduced for predicting the

flow stress evolution of multi-directionally forged commercial purity aluminum during non-isothermal annealing based on the evolution of dislocation density. In addition, the predicted flow stress for the two steps of severe plastic deformation and non-isothermal annealing were verified by experiments. Finally, the concluding remarks are summarized in Section 5.

2 Experimental

In the present study, aluminum cubes with dimensions of 15 mm × 10 mm × 10 mm were wire-cut from the as-received 1050 commercial purity aluminum billet. The specimens were isothermally annealed at 400 °C for 2 h before imposing of deformation. Then, strain magnitudes of 1, 2 and 3 were imposed by applying 2, 4 and 6 passes of multi-directional forging, respectively. In the next step, deformed specimens were annealed non-isothermally up to temperatures of 150, 200, 250, 300 and 350 °C by constant heating rate of 10 °C/min, and immediately after reaching the target temperature, specimens were quenched in water. In order to study the changes in microstructures of severely deformed and non-isothermally annealed specimens, an optical microscope was utilized. The cross sections were electro-etched by Barker solution containing 2.5 mL HBF₄ and 100 mL water. In order to evaluate the changes in the flow stress, cylinders with a height of 12 mm and a radius of 8 mm were prepared for compression test according to ASTM E9 standard from 2, 4 and 6 passes MDFed and non-isothermally annealed specimens till 150, 200, 250, 300 and 350 °C. Compression test was performed at a speed of 1 mm/min. The yield strength of the specimens is considered as the flow stress.

3 Modeling of MDF and non-isothermal annealing

3.1 ETMB model

The ETMB model which is a dislocation density-based model proposed by ESTRIN et al [25,26] for large strains is used to predict evolution of dislocation density and flow stress during MDF. In this model, the material is assumed to be a two-phase composite consisting of cell interiors as matrix with dislocation density ρ_c , and cell walls as fibers with dislocation density ρ_w . These two dislocation densities are considered as the internal variables of ETMB model. Dislocation density evolution is calculated in each phase and then dislocation density evolution of the material is calculated by the rule of mixtures. Differential equations for the evolution of dislocation density in cell interiors and cell walls are respectively as follows [34–36]:

$$\dot{\rho}_c = \alpha^* \frac{\dot{\gamma}_w \sqrt{\rho_w}}{b\sqrt{3}} - \beta^* \frac{6\dot{\gamma}_c}{bdv_c^{1/3}} - k_1 \left(\frac{\dot{\gamma}_c}{\dot{\gamma}_0} \right)^{n_1} \dot{\gamma}_c \rho_c \quad (1)$$

$$\dot{\rho}_w = \beta^* \frac{6\dot{\gamma}_c v_c^{2/3}}{bdv_w} + \beta^* \frac{\dot{\gamma}_c v_c \sqrt{3\rho_w}}{bv_w} - k_2 \left(\frac{\dot{\gamma}_w}{\dot{\gamma}_0} \right)^{n_2} \dot{\gamma}_w \rho_w \quad (2)$$

where α^* , β^* , k_1 , n_1 , k_2 and n_2 are the model parameters which are constant and irrelevant to the amount of strain; α^* is the fraction of active Frank read sources inside the cells, β^* is the fraction of dislocations inside cells with proper distance to join walls, k_1 and n_1 values are related to the dynamic recovery mechanism in cell interiors controlled by cross-slip of screw dislocations [34–36], whereas, k_2 and n_2 values are related to the dynamic recovery mechanism in cell walls controlled by the climb of edge dislocations [34–36]. Also, b and $\dot{\gamma}_0$ are the Burgers vector values of the studied material and the reference shear strain rate, respectively, $\dot{\gamma}_c$ and $\dot{\gamma}_w$ are the resolved shear strain rate in cell interiors and cell walls, respectively. In order to satisfy the strain compatibility alongside the interface between cell interiors and cell walls, the values of these two resolved shear strain rates are assumed to be equal [25,26,34–36]. Moreover, d is the cell size which should be substituted by the following equation [25,26,37–40]:

$$d = \frac{K}{\sqrt{\rho_t}} \quad (3)$$

where K is the cell size coefficient and ρ_t is the total dislocation density of material. In the early studies [25,26,37,38,41], K was considered to be constant. Later, it was modified by taking into account the effect of strain accumulation using the following equation [34,35,40,42–45]:

$$K = K_\infty + (K_0 - K_\infty) \exp(-A\gamma) \quad (4)$$

where K_0 , K_∞ and A are the model constants and γ is the local shear strain. Also, v_w and v_c in Eqs. (1) and (2) are the volume fractions of walls and cells, respectively. Note that v_w is not constant and is changed exponentially during the deformation by the following equation [34,35,37–40,42–45]:

$$v_w = v_\infty + (v_0 - v_\infty) \exp\left(\frac{\gamma}{L}\right) \quad (5)$$

where v_0 , v_∞ and L are the numerical constants. Also, volume fraction of cells can be calculated by the following equation [25,26,34]:

$$v_c = 1 - v_w \quad (6)$$

By taking into account the aforementioned points,

the differential Eqs. (1) and (2) are solved numerically in order to calculate the dislocation densities of cell interiors and cell walls, respectively. Then, based on the early assumption of material being a two-phase composite, ρ_t is calculated by rule of mixture according to the following equation [25,26,34]:

$$\rho_t = \rho_c v_c + \rho_w v_w \quad (7)$$

Eventually by calculating the total dislocation density, the flow stress is calculated by the following constitutive equation [34]:

$$\sigma_y = \sigma_0 + \alpha M G b \sqrt{\rho_t} \quad (8)$$

where σ_0 is the frictional stress of material, α is a constant, M is Taylor factor and G is the shear modulus of material.

3.2 Non-isothermal annealing model

The non-isothermal annealing model mentioned in Section 1 was based on the evolution of the unrecovered fraction of material [33]. In this study, a dislocation density-based model is presented for non-isothermal annealing in order to use the dislocation density, which is one of the outputs of ETMB model. HUMPHREYS and HATHERLY [46] suggested a differential equation for the evolution of dislocation density during recovery and formation of cell structure by the rearrangement of dislocations as follows:

$$\frac{d\rho_t}{dt} = -C_1 \rho_t^2 \quad (9)$$

where C_1 is a constant of Humphreys equation.

As it was mentioned, BORELIUS et al [29] suggested an equation for recovery based on the relaxation of stored energy of deformed material using the following equation:

$$\frac{dP}{dt} = -Pk_0 \exp\left[-\frac{Q_0 - \kappa P}{RT}\right] \quad (10)$$

where P is the stored energy of the material, T and t are the temperature and time of annealing, R is the mole gas constant and k_0 , Q_0 and κ are the equation constants which are dependent on the material being annealed, amount of pre-strain before annealing and the dominating recovery mechanism during annealing. The stored energy is proportional to the dislocation density according to the constitutive equation below [47]:

$$P = \alpha G b^2 \rho_t \quad (11)$$

By inserting constitutive Eq. (11) in Eq. (10), a new equation is achieved as follows:

$$\frac{d\rho_t}{dt} = - \left[\frac{k_0}{\rho_t} \exp \left(- \frac{Q_0 - \kappa \alpha G b^2 \rho_t}{RT} \right) \right] \rho_t^2 \quad (12)$$

By comparing Eqs. (9) and (12), C_1 is achieved as follows:

$$C_1 = - \frac{k_0}{\rho_t} \exp \left(- \frac{Q_0 - \kappa \alpha G b^2 \rho_t}{RT} \right) \quad (13)$$

In the following, the increment dt is substituted by heating rate equation, $B=dT/dt$, in Eq. (12) and a dislocation density-based differential equation for non-isothermal annealing is achieved as follows:

$$\frac{d\rho_t}{dT} = - \left[\frac{k_0}{B} \exp \left(- \frac{Q_0 - \kappa \alpha G b^2 \rho_t}{RT} \right) \right] \rho_t \quad (14)$$

To solve the differential Eq. (14) numerically, a small change of parameter κ is taken into account and it is not treated as a constant. For calculating parameter κ in each step, differential equation of unrecovered fraction [33] is used as follows:

$$\frac{dX^2}{dT} = - \frac{X^2 k_0}{B} \exp \left(- \frac{Q_0 - \omega X^2}{RT} \right) \quad (15)$$

where X is the unrecovered fraction of the material, and ω is a numerical constant. By equating the exponential terms of Eqs. (14) and (15), an equation for calculating parameter κ in each step is achieved as follows:

$$\kappa = \frac{\omega X^2}{\alpha G b^2 \rho_t} \quad (16)$$

After calculation of total dislocation density, constitutive Eq. (8) is used to track the flow stress evolutions during non-isothermal annealing.

3.3 Modeling procedure

Firstly, the dislocation densities of cell interiors and walls are calculated through Eqs. (1) and (2), respectively. Next the total dislocation density of the materials is determined using Eq. (7) in the certain amount of the accumulated strain. Using the output of ETMB model for the dislocation density as an input for the non-isothermal annealing dislocation density-based model, dislocation density evolution can be traced during the non-isothermal annealing by numerically calculating Eq. (14) and finally, flow stress evolution can be investigated through Eq. (8) for both stages of MDF and non-isothermal annealing. Values of model parameters and numerical constants are presented in Table 1. It should be noted that model constants used in this work have been verified for the same material in the previous investigations of severe plastic deformation [34,37,38,40,42–45] and non-isothermal annealing [30,33].

Table 1 Numerical constants and model parameters used in ETMB and non-isothermal annealing model [30,33,34,37,38,40,42–45]

Constant	Value	Parameter	Value
K_0	13	ρ_{c0}/m^{-2}	10^{13}
K_∞	6.5	ρ_{w0}/m^{-2}	10^{14}
A	0.26	$\dot{\gamma}_0/\text{s}^{-1}$	1
v_0	0.25	σ_0/MPa	35
v_∞	0.06	α	0.25
Γ	2.11	M	3.06
α^*	0.0024	G/GPa	26.1
β^*	0.0054	b/nm	0.286
k_1	11.5	k_0/s^{-1}	2×10^6
n_1	67	$Q_0/(\text{kJ} \cdot \text{mol}^{-1})$	124
k_2	6.9	$\omega/(\text{kJ} \cdot \text{mol}^{-1})$	36
n_2	4	$B/(\text{°C} \cdot \text{min}^{-1})$	10

4 Results and discussion

4.1 Microstructure evolution

4.1.1 MDF samples

Figure 1 shows the microstructures of pre-annealed, 2, 4 and 6 passes MDFed samples before non-isothermal annealing. As it can be seen, grain refinement happens as a result of severe plastic deformation caused by MDF and the grain size is decreased with increasing the number of MDF passes [48,49]. Also, grain morphology is changed from equiaxed to lamellar due to increasing the number of MDF passes. Since the deformation is non-uniform in the MDF process [49–51], it can be seen that grain refinement and fragmentation happen more severely in the center of the sample.

4.1.2 Two passes MDFed samples after non-isothermal annealing

Figure 2 shows the microstructures of 2 passes MDFed and non-isothermally annealed samples up to different temperatures. As can be seen, the microstructure is not affected by annealing up to 250 °C, and shear bands remain in grains and microstructure. This shows that recrystallization does not occur [46], and evolution of microstructure is probably limited to intragranular evolution such as recovery. Few small grains start to recrystallize in the microstructure at 300 °C, but unrecrystallized grains still exist in the microstructure and recrystallization process is not finished. At 350 °C, recrystallization happens completely and even some recrystallized grains experience grain growth.

4.1.3 Four passes MDFed samples after non-isothermal annealing

Figure 3 shows the microstructures of 4 passes

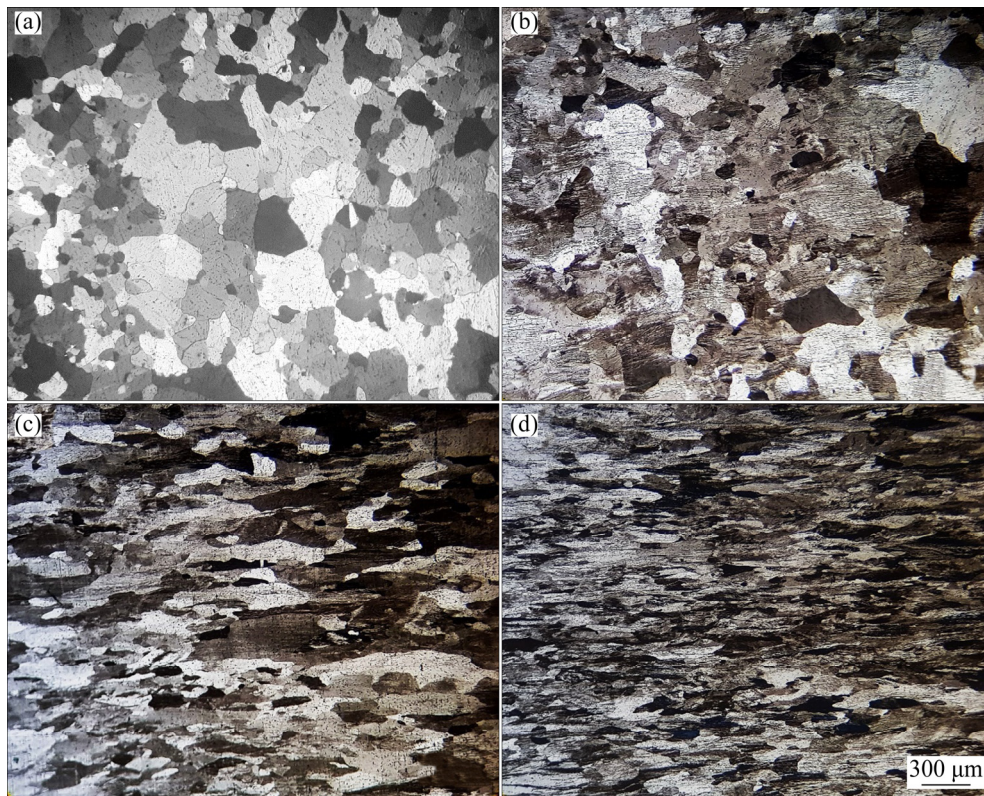


Fig. 1 Microstructures of samples before non-isothermal annealing under different conditions: (a) Pre-annealed without MDF; (b) 2 passes MDFed; (c) 4 passes MDFed; (d) 6 passes MDFed

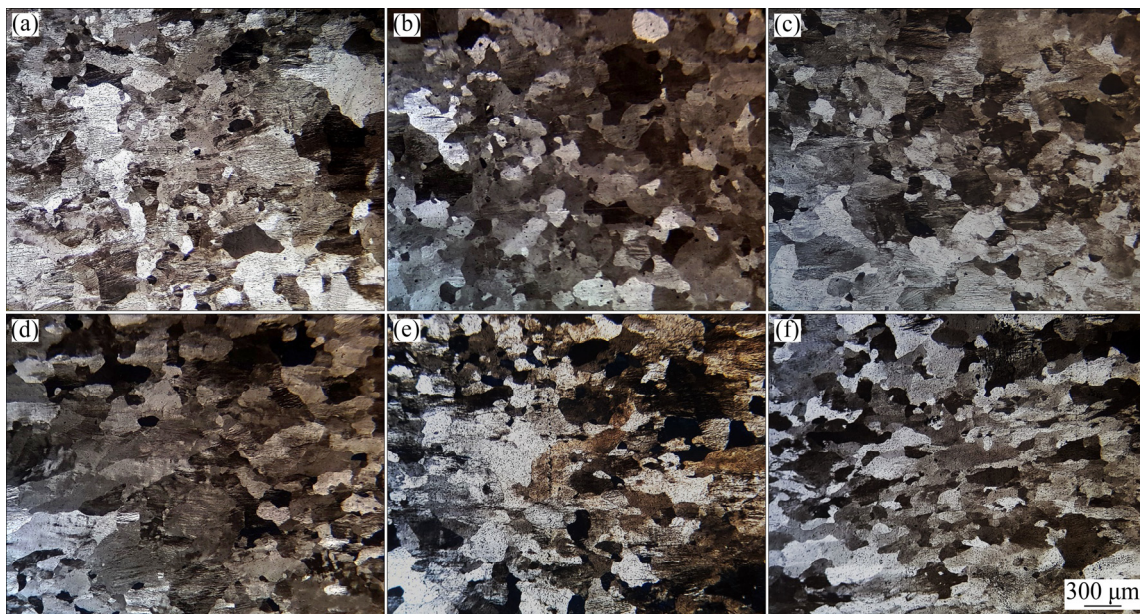


Fig. 2 Microstructures of 2 passes MDFed samples under different conditions: (a) Without annealing; (b–f) Non-isothermal annealing up to 150 °C (b), 200 °C (c), 250 °C (d), 300 °C (e) and 350 °C (f)

MDFed and non-isothermally annealed samples up to different temperatures. It can be seen that a major fraction of the microstructure changes its morphology from equiaxed to lamellar because of the increase in the amount of strain in comparison with that of 2 passes MDFed samples. Lamellar grains tend to retain during

non-isothermal annealing till 250 °C, which shows that recrystallization has not yet started and intragranular evolution is expected to happen such as dislocation rearrangements, cell structure formation and recovery. At 300 °C, a significant part of the microstructure is recrystallized and new equiaxed grains are formed, and

by continuing non-isothermal annealing up to 350 °C grain growth occurs in recrystallized grains. It seems that recrystallization starts at a temperature between 250 and 300 °C, which leads to a grain growth at 350 °C.

4.1.4 Six passes MDFed samples after non-isothermal annealing

Figure 4 shows the microstructures of 6 passes MDFed and non-isothermally annealed samples up to different temperatures. As can be seen, the morphology of grains changes from equiaxed to lamellar due to an increase in the amount of strain in comparison with those of 2 and 4 passes MDFed samples, and lamellar grains

retain their morphologies up to 300 °C. It seems that recrystallization does not happen until 300 °C in the microstructure, and recovery occurs as an intragranular evolution because of the following reasons: (1) the morphology of the grains does not change to recrystallization-induced equiaxed one, and lamellar and pancaked grains are maintained in the microstructure; (2) commercial purity aluminum has high stacking fault energy which makes it prone to occurrence of recovery during annealing [46,52]; (3) heating rate of 10 °C/min used in this study is not high enough to activate recrystallization and suppress recovery process at the

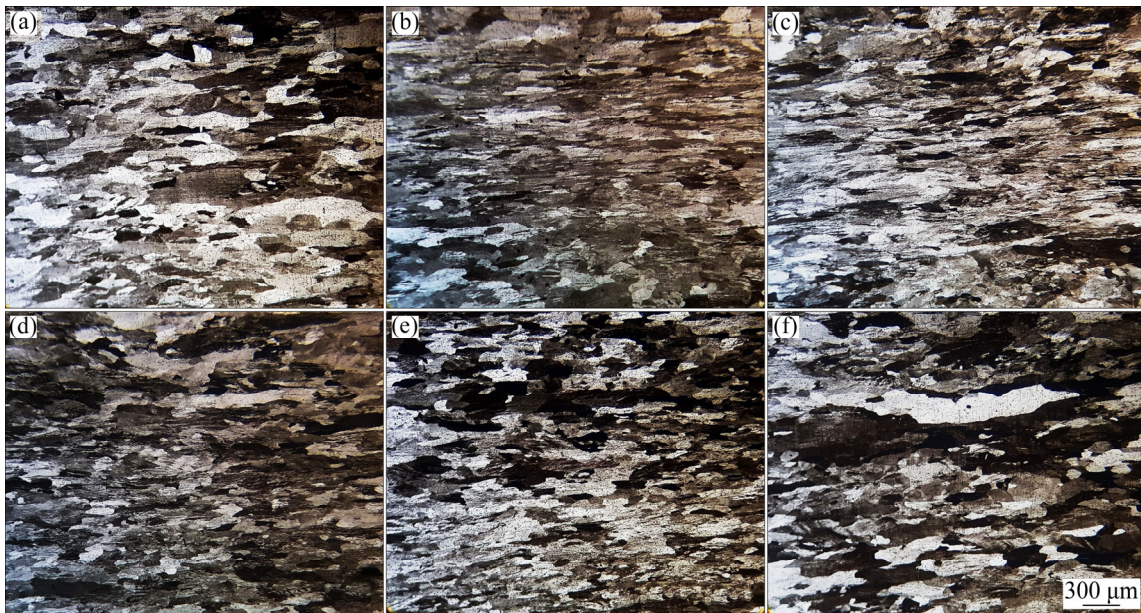


Fig. 3 Microstructures of 4 passes MDFed samples under different conditions: (a) Without annealing; (b–f) Non-isothermal annealing up to 150 °C (b), 200 °C (c), 250 °C (d), 300 °C (e) and 350 °C (f)

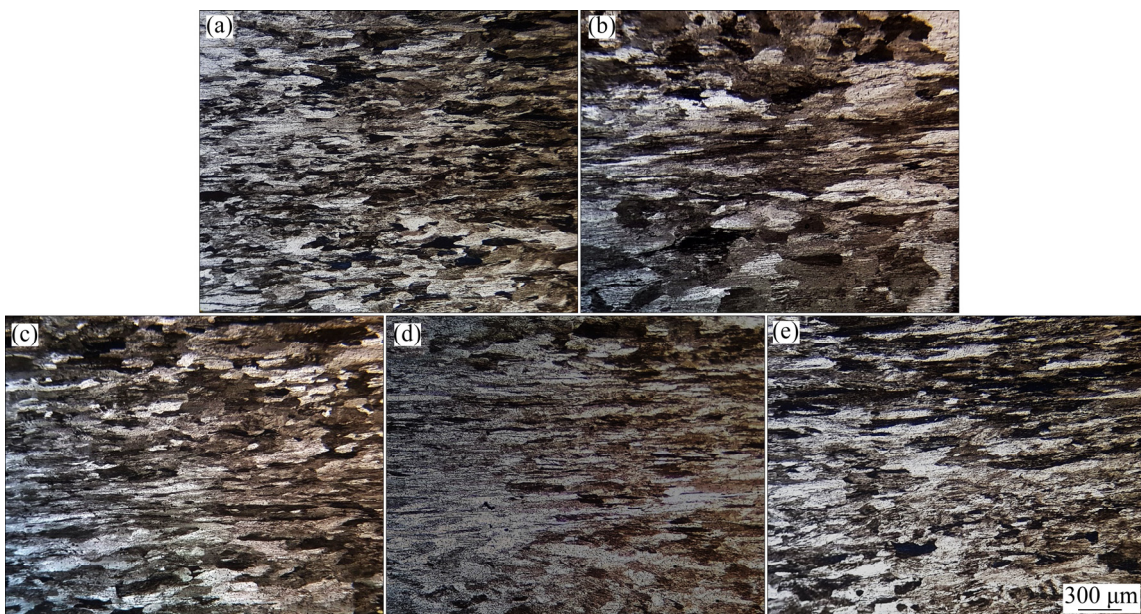


Fig. 4 Microstructures of 6 passes MDFed samples under different conditions: (a) Without annealing; (b–e) Non-isothermal annealing up to 150 °C (b), 200 °C (c), 250 °C (d) and 300 °C (e)

same time [16,18,21,53]; (4) recovery rate is increased for highly deformed materials and recovery happens more severely [8,30,54].

4.2 Modeling results

4.2.1 ETMB model

Figure 5 shows the evolution of total dislocation density versus accumulated strain of MDF process calculated by the method explained in Section 3.1. It can be seen that total dislocation density grows rapidly at lower strains due to the generation of dislocations via Frank read sources. With increasing the amount of strain, dynamic recovery occurs and the increasing rate of dislocation density reduces as it reaches a plateau at high amount of strains. As it was mentioned earlier, cross-slip of screw dislocations and climb of edge dislocations are the main mechanisms responsible for dynamic recovery in cell interiors and cell walls, respectively [34–36]. Modeling results for total dislocation density are in good agreement with earlier modeling results in Ref. [40].

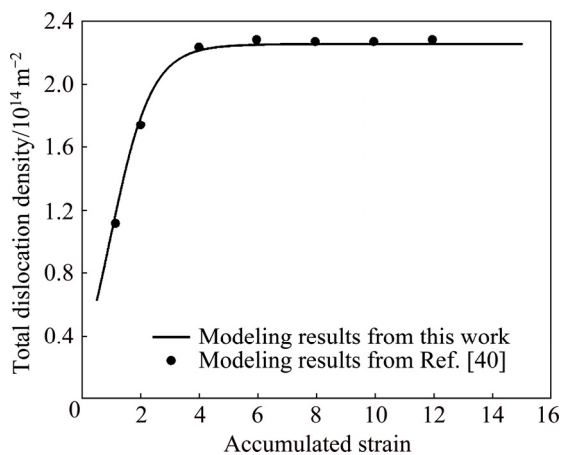


Fig. 5 Comparison of modeling results of total dislocation density from this study with modeling results in Ref. [40]

The evolution of cell size versus accumulated strain is illustrated in Fig. 6, which is calculated by Eq. (3). As can be seen, cell size decreases as a result of cell structure formation and absorption of dislocations from cell interiors to cell walls and then reaches a plateau by reaching a balance between the generation of dislocations caused by Frank read sources and annihilation of dislocations due to the dynamic recovery [25,26,34,36,40]. Modeling results for cell size are in good agreement with the earlier model in Ref. [40].

The modeling results for flow stress are also calculated by using constitutive Eq. (8) and then compared with the previous modeling results in Ref. [40] and the experimental flow stress achieved through compression tests, as shown in Fig. 7. It can be seen that the modeling results for flow stress are in good

agreement with early modeling results in Ref. [40] as well as the experimental data of flow stress. As can be seen in Fig. 7, the trend for the evolution of the flow stress follows the same pattern as the total dislocation density. At lower strains, flow stress grows rapidly. But the growth rate reduces with increasing the amount of strain, and the flow stress reaches a plateau by reaching a balance between hardening caused by the deformation and softening due to the dynamic recovery [40].

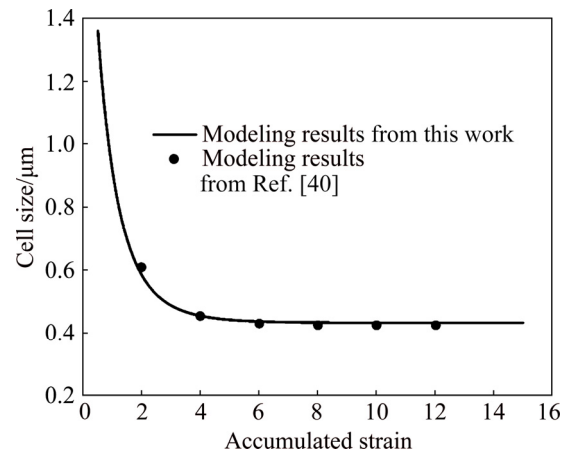


Fig. 6 Comparison of modeling results of cell size from this study with modeling results in Ref. [40]

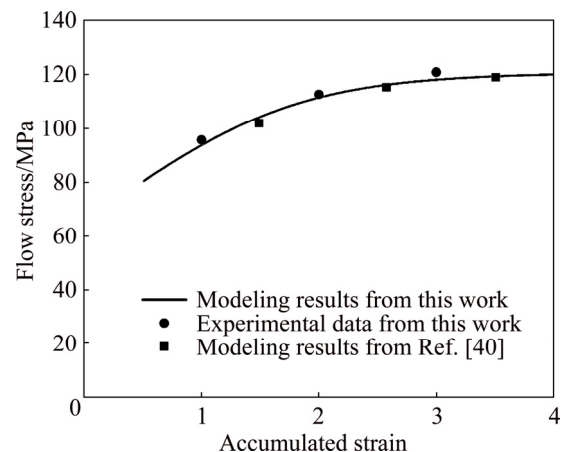


Fig. 7 Comparison of modeling results and experimental data of flow stress from this study with modeling results from Ref. [40]

4.2.2 Non-isothermal annealing model

Figure 8 shows the modeling results for total dislocation density evolution versus annealing temperature for 2, 4 and 6 passes MDFed samples. For plotting the diagrams, the total dislocation density obtained from the ETMB model at strain values of 1, 2 and 3 is used as an input for the non-isothermal annealing dislocation-based model discussed in Section 3.2. It should be noted that with increasing the number of MDF passes, the dislocation density diagrams shift to higher values, and the distance between the diagrams

reduces as the material tends to a saturation point in which dislocation density value reaches a plateau attributed to the balance between generation and annihilation of dislocations. As can be seen, all three samples have similar trend in response to annealing, the difference is that with increasing MDF passes, a plateau part becomes shorter, the reduction rate grows more intensely, and finally with increasing the magnitude of strain the samples become more sensitive towards thermally activated processes due to the increase in the stored energy and defects of the material.

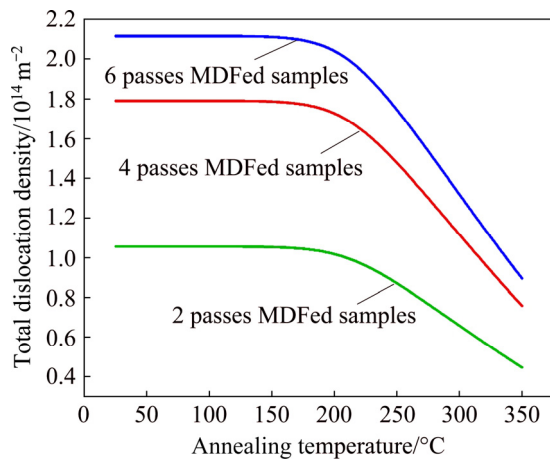


Fig. 8 Total dislocation density versus annealing temperature for 2, 4 and 6 passes MD Fed samples

Figure 9 shows the comparison between the modeling results for flow stress calculated by constitutive Eq. (8) and the experimental flow stress achieved through compression tests for 2 passes MD Fed samples non-isothermally annealed up to different temperatures. As can be seen, the model reveals a decreasing trend for the flow stress of the material. Non-isothermal annealing up to lower temperatures decreases flow stress gradually and as it was mentioned in Section 4.1.2, gradual changes are due to the occurrence of recovery in lower temperature ranges. It should be noted that as recovery occurs, it reduces the mechanical properties of the annealed material gently by a gradual trend [22,23]. At 300 °C, flow stress decreases more rapidly in comparison with the case at lower temperatures which is the consequence of the onset of recrystallization at this temperature mentioned in Section 4.1.2. A drop in the experimental flow stress is observed at 350 °C compared with the modeling results. It was discussed in Section 4.1.2 that at this temperature, the grain growth occurs in the microstructure. The proposed model is based on dislocation density evolution and the driving force for both recovery and recrystallization is dislocation density reduction, whilst the driving force for grain growth is due to the reduction of grain boundary energy. This extra decreasing factor of grain growth leads

to the drop of experimental flow stress at 350 °C in comparison with the predicted one by model. Taking into account the fact that high amount of flow stress is maintained after annealing up to 250 °C, 2 passes MD Fed sample shows acceptable thermal stability up to this temperature [3,4].

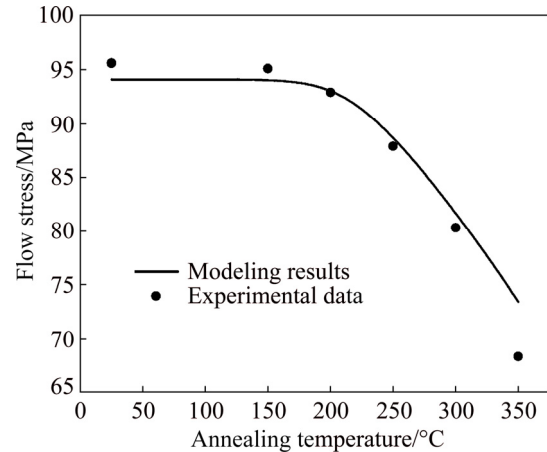


Fig. 9 Modeling results and experimental data of flow stress versus annealing temperature for 2 passes MD Fed samples

A similar pattern is observed in the experimental flow stress in comparison with modeling results for 4 passes MD Fed samples non-isothermally annealed up to different temperatures, as illustrated in Fig. 10. Non-isothermal annealing in temperature ranges lower than 250 °C decreases the flow stress gradually. By considering the non-occurrence of recrystallization up to 250 °C mentioned in Section 4.1.3, this is due to the occurrence of recovery. As mentioned in Section 4.1.3, due to the occurrence of recrystallization at 300 °C, it can be seen that the reduction rate of flow stress is severer at this temperature in comparison with that at lower temperatures. As it was mentioned in Section 4.1.3, grain growth happens at 350 °C in 4 passes MD Fed samples. Taking into account the fact that the non-

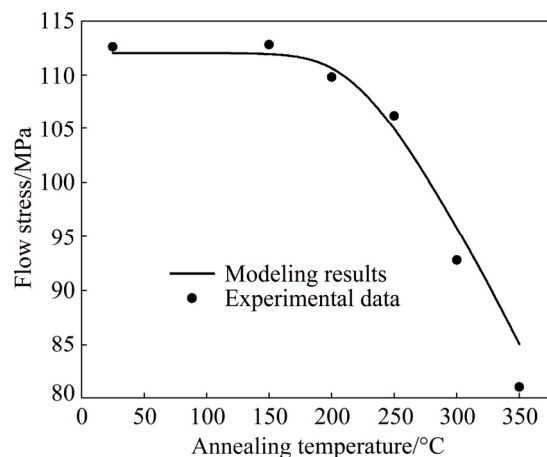


Fig. 10 Modeling results and experimental data of flow stress versus annealing temperature for 4 passes MD Fed samples

isothermal annealing model is based on dislocation density evolution and grain growth has a different driving force rather than recovery and recrystallization, the experimental flow stress at this temperature is lower than the predicted value by the model. Since the high amount of flow stress gained from MDF is maintained up to 250 °C, 4 passes MDFed samples exhibit thermal stability up to this temperature [3,4].

Figure 11 shows the modeling results for flow stress calculated by constitutive Eq. (8) compared with the experimental flow stress achieved through compression tests for 6 passes MDFed samples non-isothermally annealed up to different temperatures. It can be seen that flow stress decreases gradually by annealing up to 300 °C due to the non-occurrence of recrystallization to this temperature as mentioned in Section 4.1.4, and gradual reduction of flow stress is due to the occurrence of recovery. Imposing high amount of strains can increase both the recovery rate [3,8] and the temperature range over which the recovery takes place [3,4]. Consequently, the following outcomes are observed in this study: (1) recovery lasts up to higher temperatures in 6 passes MDFed samples in comparison with that in 2 and 4 passes MDFed samples, (2) the high amount of flow stress for 6 passes MDFed samples is preserved up to higher temperatures, and (3) the temperature range of thermal stability expands in 6 passes MDFed samples compared with that in 2 and 4 passes MDFed samples. As can be seen in Fig. 11, due to thermal stability of 6 passes MDFed samples and non-occurrence of recrystallization till 300 °C, experimental data of flow stress is higher than that predicted by Eq. (8).

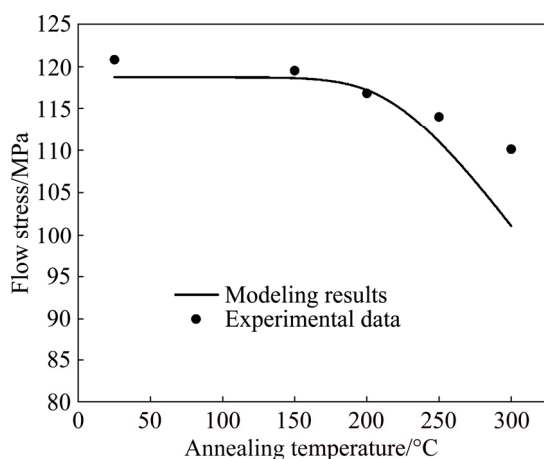


Fig. 11 Modeling results and experimental data of flow stress versus annealing temperature for 6 passes MDFed samples

5 Conclusions

(1) With increasing the number of MDF passes, the grain size reduces and the grain morphology changes from equiaxed to lamellar. Also, the yield strength is

increased and the growth rate of the yield strength is decreased.

(2) Non-isothermal annealing of 2 and 4 passes MDFed samples does not lead to recrystallization up to 250 °C. Due to the gradual reduction of flow stress as a result of recovery occurrence up to 250 °C, 2 and 4 passes MDFed samples exhibit thermal stability below 250 °C. At 300 °C, 2 passes MDFed samples experience partial recrystallization, whereas in 4 passes MDFed samples, a noticeably high fraction of microstructure is recrystallized. Non-isothermal annealing up to 350 °C leads to grain growth for 2 and 4 passes MDFed samples.

(3) Six passes MDFed samples do not experience recrystallization by non-isothermal annealing till 300 °C and exhibit thermal stability up to 300 °C due to the increasing recovery rate in high amount of strains and widening of the temperature range in which recovery happens.

(4) The experimental flow stress data are lower than the modeling results at 350 °C in 2 and 4 passes MDFed samples because of grain growth at this temperature. In the case of 6 passes MDFed sample, the experimental flow stress is higher than that predicted by the model due to thermal stability and recovery taking place up to 300 °C.

Acknowledgments

The authors wish to thank the research board of Sharif University of Technology, Iran, for the financial support and provision of the research facilities used for this work.

References

- [1] REN J, SHAN A. Strengthening and stress drop of ultrafine grain aluminum after annealing [J]. *Transactions of Nonferrous Metals Society of China*, 2010, 20: 2139–2142.
- [2] ZHAO F X, XU X C, LIU H Q, WANG Y L. Effect of annealing treatment on the microstructure and mechanical properties of ultrafine-grained aluminum [J]. *Materials & Design*, 2014, 53: 262–268.
- [3] CAO W Q, GODFREY A, HANSEN N, LIU Q. Annealing behavior of nanostructured aluminum produced by cold rolling to ultrahigh strains [J]. *Metallurgical and Materials Transactions A*, 2009, 40: 204–214.
- [4] HANSEN N, HUANG X, MØLLER M G, GODFREY A. Thermal stability of aluminum cold rolled to large strain [J]. *Journal of Materials Science*, 2008, 43: 6254–6259.
- [5] ZI A, STULIKOVA I, SMOLA B. Response of aluminum processed by extrusion preceded ECAP to isochronal annealing [J]. *Materials Science and Engineering A*, 2010, 527: 1469–1472.
- [6] YU T, HANSEN N, HUANG X. Recovery by triple junction motion in aluminium deformed to ultrahigh strains [J]. *Proceedings of the Royal Society A: Mathematical, Physical and Engineering Sciences*, 2011, 467: 3039–3065.
- [7] MISHIN O V, GODFREY A, JUUL JENSEN D, HANSEN N. Recovery and recrystallization in commercial purity aluminum cold rolled to an ultrahigh strain [J]. *Acta Materialia*, 2013, 61:

- 5354–5364.
- [8] YU T, HANSEN N, HUANG X. Linking recovery and recrystallization through triple junction motion in aluminum cold rolled to a large strain [J]. *Acta Materialia*, 2013, 61: 6577–6586.
- [9] YU C Y, SUN P L, KAO P W, CHANG C P. Evolution of microstructure during annealing of a severely deformed aluminum [J]. *Materials Science and Engineering A*, 2004, 366: 310–317.
- [10] FERRASSE S, SEGAL V M, ALFORD F. Texture evolution during equal channel angular extrusion (ECAE) [J]. *Materials Science and Engineering A*, 2004, 372: 235–244.
- [11] CAO W Q, GODFREY A, LIU W, LIU Q. Annealing behavior of aluminium deformed by equal channel angular pressing [J]. *Materials Letters*, 2003, 57: 3767–3774.
- [12] CAO W Q, GODFREY A, LIU W, LIU Q. EBSD study of the annealing behavior of aluminum deformed by equal channel angular processing [J]. *Materials Science and Engineering A*, 2003, 360: 420–425.
- [13] KWAN C, WANG Z, KANG S B. Mechanical behavior and microstructural evolution upon annealing of the accumulative roll-bonding (ARB) processed Al alloy 1100 [J]. *Materials Science and Engineering A*, 2008, 480: 148–159.
- [14] MOGHANAKI S K, KAZEMINEZHAD M, LOGÉ R. Heating rate effect on particle stimulated nucleation and grains structure during non-isothermal annealing of multi-directionally forged solution treated AA2024 [J]. *Materials Characterization*, 2017, 127: 317–324.
- [15] POORGANJI B, SEPEHRBAND P, JIN H, ESMAEILI S. Effect of cold work and non-isothermal annealing on the recrystallization behavior and texture evolution of a precipitation-hardenable aluminum alloy [J]. *Scripta Materialia*, 2010, 63: 1157–1160.
- [16] SCHÄFER C, MOHLES V, GOTTSSTEIN G. Modeling the effect of heating rate on recrystallization texture evolution in AA3103 [J]. *Advanced Engineering Materials*, 2010, 12: 981–988.
- [17] SUN N, PATTERSON R B, SUNI P J, DOHERTY D R, WEILAND H, KADOLKAR P, BLUE A C, THOMPSON B G. Effect of heating rate on recrystallization of twin roll cast aluminum [J]. *Metallurgical and Materials Transactions A*, 2008, 39: 165–170.
- [18] SHEN F, WANG B, YI D, LIU H, TANG C, SHOU W. Effects of heating rate during solid-solution treatment on microstructure and fatigue properties of AA2524 T3 Al–Cu–Mg sheet [J]. *Materials & Design*, 2016, 104: 116–125.
- [19] KHANI MOGHANAKI S, KAZEMINEZHAD M, LOGÉ R. Effect of concurrent precipitation on the texture evolution during continuous heating of multi directionally forged solution treated Al–Cu–Mg alloy [J]. *Materials Characterization*, 2017, 131: 399–405.
- [20] ATTALLAH M M, STRANGWOOD M, DAVIS C L. Influence of the heating rate on the initiation of primary recrystallization in a deformed Al–Mg alloy [J]. *Scripta Materialia*, 2010, 63: 371–374.
- [21] SEPEHRBAND P, WANG X, JIN H, ESMAEILI S. Microstructural evolution during non-isothermal annealing of a precipitation-hardenable aluminum alloy: Experiment and simulation [J]. *Acta Materialia*, 2015, 94: 111–123.
- [22] XIA S L, MA M, ZHANG J X, WANG W X, LIU W C. Effect of heating rate on the microstructure, texture and tensile properties of continuous cast AA 5083 aluminum alloy [J]. *Materials Science and Engineering A*, 2014, 609: 168–176.
- [23] SUMMERS P T, CASE S W, LATTIMER B Y. Residual mechanical properties of aluminum alloys AA5083-H116 and AA6061-T651 after fire [J]. *Engineering Structures*, 2014, 76: 49–61.
- [24] KHANI MOGHANAKI S, KAZEMINEZHAD M, LOGÉ R. Recrystallization behavior of multi-directionally forged over-aged and solution treated Al–Cu–Mg alloy during non-isothermal annealing [J]. *Materials & Design*, 2017, 132: 250–256.
- [25] ESTRIN Y, TÓTH L S, MOLINARI A, BRÉCHET Y. A dislocation-based model for all hardening stages in large strain deformation [J]. *Acta Materialia*, 1998, 46: 5509–5522.
- [26] TOTH L S, MOLINARI A, ESTRIN Y. Strain hardening at large strains as predicted by dislocation based polycrystal plasticity model [J]. *Journal of Engineering Materials and Technology*, 2002, 124: 71–77.
- [27] KUHLMANN D, MASING G, RAFFELSIEPER J. On the theory of recovery [J]. *Zeitschrift Fur Metallkunde*, 1949, 40: 241–246.
- [28] NES E. Recovery revisited [J]. *Acta Metallurgica et Materialia*, 1995, 43: 2189–2207.
- [29] BORELIUS G, BERGLUND S, SJOBERG S. Measurements on the evolution of heat during the recovery of cold-worked metals [J]. *Arkiv For Fysik*, 1953, 6: 143–149.
- [30] VANDERMEER R A, HANSEN N. Recovery kinetics of nanostructured aluminum: Model and experiment [J]. *Acta Materialia*, 2008, 56: 5719–5727.
- [31] YU T B, HANSEN N. Recovery kinetics in commercial purity aluminum deformed to ultrahigh strain: Model and experiment [J]. *Metallurgical and Materials Transactions A*, 2016, 47: 4189–4196.
- [32] YU T B, HANSEN N. A model for recovery kinetics of aluminum after large strain [J]. *Materials Science Forum*, 2012, 715–716: 374–379.
- [33] SUMMERS P T, MOURITZ A P, CASE S W, LATTIMER B Y. Microstructure-based modeling of residual yield strength and strain hardening after fire exposure of aluminum alloy 5083-H116 [J]. *Materials Science and Engineering A*, 2015, 632: 14–28.
- [34] HOSSEINI E, KAZEMINEZHAD M. A hybrid model on severe plastic deformation of copper [J]. *Computational Materials Science*, 2009, 44: 1107–1115.
- [35] HOSSEINI E, KAZEMINEZHAD M. ETMB model investigation of flow softening during severe plastic deformation [J]. *Computational Materials Science*, 2009, 46: 902–905.
- [36] KAZEMINEZHAD M, HOSSEINI E. Modeling of induced empirical constitutive relations on materials with FCC, BCC, and HCP crystalline structures: Severe plastic deformation [J]. *International Journal of Advanced Manufacturing Technology*, 2010, 47: 1033–1039.
- [37] TÓTH L S. Modelling of strain hardening and microstructural evolution in equal channel angular extrusion [J]. *Computational Materials Science*, 2005, 32: 568–576.
- [38] BAIK S C, ESTRIN Y, KIM H S, HELLMIG R J. Dislocation density-based modeling of deformation behavior of aluminium under equal channel angular pressing [J]. *Materials Science and Engineering A*, 2003, 351: 86–97.
- [39] KAZEMINEZHAD M, HOSSEINI E. Coupling kinetic dislocation model and Monte Carlo algorithm for recrystallized microstructure modeling of severely deformed copper [J]. *Journal of Materials Science*, 2008, 43: 6081–6086.
- [40] HOSSEINI E, KAZEMINEZHAD M. The effect of ECAP die shape on nano-structure of materials [J]. *Computational Materials Science*, 2009, 44: 962–967.
- [41] MCKENZIE P W J, LAPOVOK R, ESTRIN Y. The influence of back pressure on ECAP processed AA6016: Modeling and experiment [J]. *Acta Materialia*, 2007, 55: 2985–2993.
- [42] HOSSEINI E, KAZEMINEZHAD M. Dislocation structure and strength evolution of heavily deformed tantalum [J]. *International Journal of Refractory Metals and Hard Materials*, 2009, 27: 605–610.
- [43] HOSSEINI E, KAZEMINEZHAD M, MANI A, RAFIZADEH E. On the evolution of flow stress during constrained groove pressing of pure copper sheet [J]. *Computational Materials Science*, 2009, 45: 855–859.
- [44] PARVIN H, KAZEMINEZHAD M. Development of a dislocation density based model considering the effect of stacking fault energy: Severe plastic deformation [J]. *Computational Materials Science*,

- 2014, 95: 250–255.
- [45] ESTRIN Y, MOLOTNIKOV A, DAVIES C H J, LAPOVOK R. Strain gradient plasticity modelling of high-pressure torsion [J]. *Journal of the Mechanics and Physics of Solids*, 2008, 56: 1186–1202.
- [46] HUMPHREYS F J, HATHERLY M. *Recrystallization and related annealing phenomena* [M]. 2nd ed. Amsterdam: Elsevier, 2004.
- [47] GODFREY A, CAO W Q, LIU Q, HANSEN N. Stored energy, microstructure, and flow stress of deformed metals [J]. *Metallurgical and Materials Transactions A*, 2005, 36: 2371–2378.
- [48] ZHU Q F, WANG W J, ZHAO Z H, ZUO Y B, CUI J Z. Effect of multi-forging condition on deformed structure and mechanical properties of a 99.995 percent high purity aluminum [J]. *Materials Science Forum*, 2015, 817: 360–366.
- [49] ZHU Q, LI L, BAN C, ZHAO Z, ZUO Y, CUI J. Structure uniformity and limits of grain refinement of high purity aluminum during multi-directional forging process at room temperature [J]. *Transactions of Nonferrous Metals Society of China*, 2014, 24: 1301–1306.
- [50] VALIEV R Z, ESTRIN Y, HORITA Z, LANGDON T G, ZECHETBAUER M J, ZHU Y T. Producing bulk ultrafine-grained materials by severe plastic deformation [J]. *JOM*, 2006, 58: 33–39.
- [51] GUPTA R, PANTHI S K, SRIVASTAVA S. Assessment of various properties evolved during grain refinement through multi-directional forging [J]. *Reviews on Advanced Materials Science*, 2016, 46: 70–85.
- [52] HUMPHREYS F J. A unified theory of recovery, recrystallization and grain growth, based on the stability and growth of cellular microstructures—I. The basic model [J]. *Acta Materialia*, 1997, 45: 4231–4240.
- [53] ATKINSON M. On the credibility of ultra rapid annealing [J]. *Materials Science and Engineering A*, 2003, 354: 40–47.
- [54] FURU T, ØRSUND R, NES E. Subgrain growth in heavily deformed aluminium—Experimental investigation and modelling treatment [J]. *Acta Metallurgica et Materialia*, 1995, 43: 2209–2232.

非等温退火对大变形铝试样组织和力学性能的影响：模拟与实验

A. R. KHODABAKHSHI, M. KAZEMINEZHAD

Department of Materials Science and Engineering, Sharif University of Technology, Azadi Avenue, Tehran, Iran

摘要：为了研究铝在非等温退火过程中的组织演变和流动应力，分别采用 2、4 和 6 道次多向锻造工艺，使试样应变量为 1、2 和 3。然后，在 150、200、250、300 和 350 °C 下对试样进行非等温退火。通过对变形阶段和退火阶段的模拟，研究位错密度和流动应力的演化规律。结果发现，经 2、4 和 6 道次多向锻造的试样在温度分别达到 250、250 和 300 °C 时其热稳定性仍然较好。模拟结果与实验数据吻合较好。与模拟得到的流动应力值相比，经 2 道次和 4 道次多向锻造的样品在 350 °C 非等温退火后的实验流动应力值偏低。其根本原因在于，模拟所用非等温退火模型仅是基于晶内位错密度演化，只考虑了回复和再结晶现象；然而，在 350 °C 退火后，除了回复和再结晶外，还会发生晶粒长大现象，这使得模拟和实验得到的流动应力值出现偏差。

关键词：大塑性变形；多向锻造；非等温退火；位错密度模型；显微组织；力学性能

(Edited by Wei-ping CHEN)